Microfluid Nanofluid (2010) 9:1103–1114
DOI 10.1007/s10404-010-0631-2

RESEARCH PAPER

# Comparative study between computational and experimental results for binary rarefied gas flows through long microchannels

**Lajos Szalmas · Jeerasak Pitakarnnop · Sandrine Geoffroy · Stephane Colin · Dimitris Valougeorgis**

Received: 18 February 2010 / Accepted: 19 April 2010 / Published online: 21 May 2010


**Abstract** A comparative study between computational and experimental results for pressure-driven binary gas flows through long microchannels is performed. The theoretical formulation is based on the McCormack kinetic model and the computational results are valid in the whole range of the Knudsen number. Diffusion effects are taken into consideration. The experimental work is based on the Constant Volume Method, and the results are in the slip and transition regime. Using both approaches, the molar flow rates of the He–Ar gas mixture flowing through a rectangular microchannel are estimated for a wide range of pressure drops between the upstream and downstream reservoirs and several mixture concentrations varying from pure He to pure Ar. In all cases, a very good agreement is found, within the margins of the introduced modeling and measurement uncertainties. In addition, computational results for the pressure and concentration distributions along the channel are provided. As far as the authors are aware of, this is the first detailed and complete comparative study between theory and experiment for gaseous flows through long microchannels in the case of binary mixtures.

**Keywords** Binary rarefied gas flows · McCormack model · Discrete velocity method · Flow rate measurement

L. Szalmas · D. Valougeorgis (✉)
Department of Mechanical Engineering, University of Thessaly, 38334 Pedion Areos, Volos, Greece
e-mail: diva@mie.uth.gr

L. Szalmas
e-mail: lszalmas@gmail.com

J. Pitakarnnop · S. Geoffroy · S. Colin
INSA, UPS, Mines Albi, ISAE, ICA (Institut Clément Ader), Université de Toulouse, 135 avenue de Rangueil, 31077 Toulouse, France
e-mail: pitakarnnop_j@hotmail.com

S. Geoffroy
e-mail: sandrine.geoffroy@insa-toulouse.fr

S. Colin
e-mail: stephane.colin@insa-toulouse.fr

## 1 Introduction

During the last decade, rarefied gas flows through long channels have attracted considerable attention. This increasing interest has been mainly stimulated by their wide applicability in various technological fields including the emerging field of nano- and microfluidics (Ho and Tai 1998; Kandlikar et al. 2006). In order to understand such flows, both theoretical and experimental studies have been carried out.

From theoretical standpoint, the most commonly applied approaches include extended hydrodynamics (Colin 2005; Szalmas 2007; Morini et al. 2005; Pitakarnnop et al. 2008; Lockerby and Reese 2008), the DSMC method (Bird 1994), and kinetic theory, as specified by the Boltzmann equation or alternatively by reliable kinetic model equations (Ferziger and Kaper 1972; Cercignani 1988; Sharipov and Seleznev 1998). It has been shown that for flows with small Mach numbers (such as the ones investigated here) and the Knudsen number varying from the free molecular through the transition up to the hydrodynamic regimes, linearized kinetic theory is the most efficient approach providing reliable results with modest computational effort. The discrete velocity method has been successfully developed for solving such kinetic equations, simulating flows through long channels of various cross sections for both single component gases

(Sharipov 1999; Aoki 2001; Valougeorgis and Naris 2003; Breyiannis et al. 2008) and gaseous mixtures (Sharipov and Kalempa 2002; Takata et al. 2003; Naris et al. 2004, 2005; Kosuge and Takata 2008). In addition, in the case of one-dimensional flows the semi-analytical discrete ordinate method has been developed to solve kinetic equations associated with gaseous mixtures in a very elegant and computationally efficient manner (Siewert and Valougeorgis 2004).

The experimental work for flows through long channels has been based mainly on the Constant Volume and the Droplet Tracking methods. By implementing the corresponding test rigs, flow rates through various channels have been measured (Harley et al. 1995; Zohar et al. 2002; Maurer et al. 2003; Colin et al. 2004; Ewart et al. 2006, 2007; Marino 2009; Pitakarnnop et al. 2010). All those studies, which also include comparisons between theory and experiments, as well as efforts for estimating the accommodation coefficients characterizing the gas-surface interaction, have been focused on single component gases. Recently, one of these studies has been applied to binary gaseous mixtures (Pitakarnnop et al. 2010), where an introductory comparison between theory and experiment has been performed. However, in this latter study, the comparison has been limited to $Kn < 0.05$, and also, it has been based on the measured and computed mass flow rates and not on the molar flow rates, which as described later, in the case of binary mixture flows, remain the proper quantity for comparisons between computational and experimental results.

In that framework, in this study, a detailed and systematic comparison between computational and experimental results for binary gas flows through long microchannels is performed in the slip and transition regimes. In particular, the flow configuration under investigation includes the gaseous mixture of He–Ar flowing through a rectangular microchannel for a wide range of pressure drops between the upstream and downstream reservoirs and several mixture concentrations varying from pure He to pure Ar. The comparative study is based on the computed and measured molar flow rates. The diffusion effects including the concentration variation along the channel are also considered in the computations, and for several indicative cases, pressure and concentration distributions along the channel are provided.

In Sect. 2, the definition of the problem under investigation is given, followed by the description of the computational formulation and the experimental setup as detailed in Sects. 3 and 4, respectively. In Sect. 5, the comparative study based on the computed and measured flow rates is presented, supplemented by some complementary computational results. Finally, concluding remarks are presented in Sect. 6.

## 2 Definition of the problem

The isothermal pressure-driven flow of a binary gas mixture through a microchannel, connecting two reservoirs, is considered. The channel has rectangular cross section with height $H = 1.88$ μm, width $W = 21.2$ μm, and length $L = 5000$ μm, with $H$ being the characteristic length. Since $H, W \ll L$, end effects at the inlet and outlet of the channel may be neglected. The channel axis lies in the $z'$ direction, while the cross section is in the $x'$, $y'$ coordinate sheet.

The gas mixture is consisting of two species, namely He and Ar, having molecular masses $m_1 = 0.004003$ kg/mol and $m_2 = 0.03995$ kg/mol, respectively. The concentration of the light species in the gas mixture is defined by

$$C(z') = \frac{n_1(z')}{n_1(z') + n_2(z')}, \tag{1}$$

where $n_\alpha(z')$, with $\alpha = 1, 2$, denotes the molar density of the two species, while $n = n_1 + n_2$ is the molar density of the mixture. Index 1 refers always to He, since it is the lighter gas compared to Ar. Also, from now on, we will refer to $C$ as the concentration of the gas mixture. Furthermore, the molecular mass of the mixture is defined by

$$m(C) = Cm_1 + (1 - C)m_2. \tag{2}$$

Other quantities of the mixture of some importance in this study are its viscosity $\mu(C)$ and the characteristic molecular speed of the mixture $v(C) = \sqrt{2kT/m(C)}$, where $k = 1.3807 \times 10^{-23}$ J/K is the Boltzmann constant and $T$ a constant temperature characterizing the isothermal flow. Also, the pressure of the mixture along the channel is given by the equation of state

$$P(z') = n(z')kT. \tag{3}$$

It is seen that all quantities specified in this paragraph (except $m_1$, $m_2$, and $T$) depend explicitly or implicitly on $z'$ and, therefore, vary in the flow direction.

The pressure and concentration of the gas mixture in the reservoirs are defined as ($P_A$, $C_A$) and ($P_B$, $C_B$), with the indexes $A$ and $B$ denoting the upstream and downstream reservoirs, respectively. In this study, the flow is purely due to an externally imposed pressure gradient and, therefore, $P_A > P_B$, while $C_A = C_B$. The concentration $C_A$ is taken as the reference concentration of the gas mixture. It is emphasized, that although the concentration of the mixture at the two reservoirs is the same, a variation of the mixture concentration along the channel may appear due to the fact that the particles of the two species are traveling with different molecular speeds. This phenomenon, known as separation effect, has been discussed in the past by several authors (Sharipov and Kalempa 2005; Takata et al. 2007; Szalmas and Valougeorgis 2010). It is also noted that during the flow process the concentration of the mixture in

the reservoirs is considered as constant, since the number of gas molecules flowing through the channel is negligible compared to the gas molecules in the reservoirs.

Based on the above, the local dimensionless pressure and concentration gradients are defined as

$$X_P = \frac{H}{P}\frac{\partial P}{\partial z'} \quad \text{and} \quad X_C = \frac{H}{C}\frac{\partial C}{\partial z'}, \tag{4}$$

respectively.

A very important flow parameter is the local rarefaction parameter given by

$$\delta = \frac{P(z')H}{\mu(C)v(C)}, \tag{5}$$

with $P_A \leq P(z') \leq P_B$. The rarefaction parameter varies along the channel between the rarefaction parameters in the upstream and downstream reservoirs, denoted by $\delta_A$ and $\delta_B$, respectively. In general, the rarefaction parameter is proportional to the inverse Knudsen number. For the purposes of this study, the reference rarefaction parameter, $\delta_0 = (\delta_A + \delta_B)/2$ and the corresponding Knudsen number, $Kn_0 = 1/\delta_0$, are defined. As is seen from the definition of $\delta$, the Knudsen number is defined in terms of the channel height $H$, while the mean free path is defined via the mixture viscosity $\mu(C)$.

The quantity of major importance in this study, upon which the comparison study between theory and experiment is based, is the total molar flow rate defined as

$$J = J_1 + J_2, \tag{6}$$

which consists of the sum of the molar flow rates $J_1$ and $J_2$ of He and Ar, respectively. The molar flow rates of each species are given by the integrals

$$J_\alpha = n_\alpha(z') \iint_{A'} u'_\alpha(x', y')\mathrm{d}x'\mathrm{d}y', \tag{7}$$

with $\alpha = 1, 2$, where $u'_\alpha(x', y')$ is the macroscopic velocity, and $A' = H \times W$ is the area of the cross section. It is seen, from Eq. 7, that the molar flow rates correspond to the amount of molecules in mol unit passing through a cross section of the channel per unit time. It is emphasized that although, at the right-hand side of Eq. 7, the molar density and the integral term vary along the flow, their product and, therefore, the molar flow rates $J_1$, $J_2$, and $J$, due to particle conservation, remain invariant at each cross section. In the flow configuration presented here, this invariance of the molar flow rates at each cross section is always satisfied.

## 3 Computational approach

The solution of the flow of a binary gas mixture through a channel of rectangular cross section has been obtained in Naris et al. (2005) in the whole range of the Knudsen number based on the McCormack kinetic model (McCormack 1973). This model is considered as a reliable alternative of the Boltzmann equation, since it satisfies all collision invariants, fulfills the H-theorem, and provides the correct expressions for all transport coefficients. It is also noted that while solving the viscous slip problem for binary gas mixtures, very good agreement has been found between the corresponding solutions of the linearized Boltzmann equation (Ivchenko et al. 1997) and of the McCormack model (Sharipov and Kalempa 2003) (see Table 2 in Sharipov and Kalempa (2003)). Of course, it is clarified that, strictly speaking, the present theoretical/computational study is valid for monatomic dilute gas mixtures, which is also the case for the Boltzmann equation. This description is well suited for rarefied gases. For the flow under consideration, i.e., binary gas flow through a rectangular channel an advanced discrete velocity algorithm (Naris et al. 2004a, b) has been applied in Naris et al. (2005) to solve the resulting system of linear integro-differential equations. The results are in dimensionless form and include the so-called kinetic coefficients.

In this study, the kinetic coefficients for the specific geometry, data and parameters imposed in the present flow configuration are computed. It is emphasized that the realistic potential (Kestin et al. 1984; Naris et al. 2004b, 2005) is chosen for the computations. This model ensures the correct value of the binary gas mixture viscosity, which has been defined by applying the Chapman-Enskog theory to the McCormack model (Sharipov and Kalempa 2002). Furthermore, for the needs of this study, a methodology has been developed to convert the dimensionless results into dimensional molar flow rates, taking into account the variation of the flow quantities, including diffusion effects, along the channel.

To start with, the molar flow rates $J_P$ and $J_C$ conjugated to the local gradients $X_P$ and $X_C$ are introduced as (De Groot and Mazut 1984; Sharipov and Kalempa 2002)

$$J_P = -n \iint_{A'} w\mathrm{d}x'\mathrm{d}y', \tag{8}$$

$$J_C = -n_1 \iint_{A'} \left(u'_1 - u'_2\right)\mathrm{d}x'\mathrm{d}y', \tag{9}$$

where

$$w(x', y') = \frac{n_1 u'_1 + n_2 u'_2}{n_1 + n_2} \tag{10}$$

is the averaged velocity. Also, it is noted that $J_P$ and $J_C$ are connected to the pressure and concentration gradients according to (Sharipov and Kalempa 2002; Naris et al. 2005)

$$J_P = \frac{nA'v(C)}{2}[\Lambda_{PP}X_P + \Lambda_{PC}X_C], \tag{11}$$

$$J_C = \frac{nA'v(C)}{2}[\Lambda_{CP}X_P + \Lambda_{CC}X_C], \tag{12}$$

where $\Lambda_{PP}$, $\Lambda_{CP}$, $\Lambda_{PC}$, and $\Lambda_{CC}$, with $\Lambda_{CP} = \Lambda_{PC}$ due to the Onsager-Casimir relation, are the kinetic coefficients (Sharipov 1994). The kinetic formulation on the basis of $J_P$ and $J_C$ provides a theoretically well-established and convenient way of the problem definition.

It is useful to point that, in the formulation which follows, all four kinetic coefficients, which may contribute to the calculation of the molar flow rates $J_1$ and $J_2$ are considered. In particular, the coefficients $\Lambda_{PP}$ and $\Lambda_{CP}$ are due to the externally imposed pressure gradient, while the coefficients $\Lambda_{PC}$ and $\Lambda_{CC}$ are due to a concentration gradient along the channel, which is not externally imposed but is developed due to separation.

Using Eqs. 8–10 and the definition of the molar flow rates $J_\alpha$, $\alpha = 1, 2$, given in Eq. 7, it is readily seen that

$$J_1 = -CJ_P - (1-C)J_C, \tag{13}$$

$$J_2 = -(1-C)(J_P - J_C). \tag{14}$$

Combining these expressions with Eqs. 11 and 12 and using the ideal gas law (see Eq. 3), the following system of equations is obtained (Szalmas and Valougeorgis 2010):

$$J_1 = -\frac{PA'H}{m(C)v(C)L}\left[(C\Lambda_{PP} + (1-C)\Lambda_{CP})\frac{\partial P}{\partial \hat{z}}\frac{1}{P} + (C\Lambda_{PC} + (1-C)\Lambda_{CC})\frac{\partial C}{\partial \hat{z}}\frac{1}{C}\right], \tag{15}$$

$$J_2 = -\frac{PA'H}{m(C)v(C)L}(1-C)\left[(\Lambda_{PP} - \Lambda_{CP})\frac{\partial P}{\partial \hat{z}}\frac{1}{P} + (\Lambda_{PC} - \Lambda_{CC})\frac{\partial C}{\partial \hat{z}}\frac{1}{C}\right], \tag{16}$$

where, $0 \le \hat{z} \le 1$, defined by $\hat{z} = z'/L$, is the non-dimensional coordinate along the axis of the channel. These equations are supplemented with the boundary conditions for the pressure and the concentration at the inlet and the outlet of the channel:

$$P(0) = P_A, \quad P(1) = P_B, \tag{17}$$

$$C(0) = C_A, \quad C(1) = C_B. \tag{18}$$

Equations 15 and 16 constitute a nonlinear system of two first-order ordinary differential equations, subject to (17) and (18). It can be solved to yield the unknown axial distributions $P = P(\hat{z})$ and $C = C(\hat{z})$, while the unknown flow rates $J_\alpha$ are defined by satisfying the conditions at $\hat{z} = 1$.

Finally, the solution of Eqs. 15 and 16 is carried out numerically. Initial estimates of $J_1$ and $J_2$ are provided and then the system is solved by the Euler's method, starting from $\hat{z} = 0$ and marching with a discrete step $\Delta\hat{z}$ up to $\hat{z} = 1$. At each node along the channel, based on the values of the kinetic coefficients of the previous node, the values of $P$ and $C$ are estimated. Reaching the end of the channel at $\hat{z} = 1$, the computed values of the pressure and the concentration are compared to the corresponding boundary conditions. If the agreement is not satisfactory, then updated values of $J_1$ and $J_2$ based on the bisector method are provided, and the solution of the system is repeated. This iteration process terminates when some relative convergence criterion imposed on the outlet pressure and concentration is satisfied. Upon convergence, the distributions $P(\hat{z})$ and $C(\hat{z})$, as well as the quantities $J_1$ and $J_2$ are determined. Finally, the total flow rate $J$ is calculated from $J_\alpha$ using Eq. 6.

As we conclude this section, the discretization parameters implemented in the computations are provided. The numerical algorithm used for the computation of the kinetic coefficients in Eqs. 15 and 16 is based on a computational grid consisting of 201 × 201 nodes for $Kn_0 \ge 1$, and 301 × 301 nodes for $Kn_0 < 1$ in the physical space, and of 64 magnitudes and 280 polar angles for all Knudsen numbers in the molecular velocity space. The iteration process for the estimation of the kinetic coefficients is terminated when the relative convergence error is less than $10^{-7}$. Also, the Euler method involved in the solution of Eqs. 15 and 16 is based on a marching step of $\hat{z} = 1/500$, while the convergence criterion imposed on the outlet pressure and concentration is equal to $10^{-6}$. Based on the above discretization, the results thus obtained are considered as accurate up to at least three significant figures.

## 4 Experimental approach

All the experimental data are obtained from an experimental setup described in Pitakarnnop et al. (2010), using the so-called Constant Volume Method. The microsystem is composed of a series of 45 identical microchannels etched by deep reactive ion etching (DRIE) in a silicon wafer, and closed by anodic bonding with a Pyrex plate. The height of the microchannels, $H = 1.88$ μm, has been measured by a TENCOR P1 profilometer, and the initial uncertainty of ±0.1 μm was finally reduced to ±0.01 μm, after comparison between measured and simulated flow rates in the hydrodynamic regime, at low Knudsen numbers (Colin et al. 2004). The width of the microchannels is $W = 21.2 \pm 0.3$ μm, and their length is $L = 5000 \pm 10$ μm. The microchannels are connected to large upstream and downstream reservoirs, the constant volumes of which have been accurately measured using a specific setup, with an accuracy of ±1.3%. During the flow of the gas through the

microsystem, the pressure inside each reservoir is measured by means of Inficon® capacitance diaphragm gauges, and the molar flow rates can be deduced from the ideal gas equation of state. The accuracy of the pressure measurements by the capacitance pressure gauges is 0.2% of reading. In order to maintain isothermal conditions, the setup is thermally regulated by two Peltier modules, which allow maintaining a constant and uniform temperature inside the whole setup, i.e., inside the reservoirs as well as around the microsystem and all the connecting lines. Before each experiment, the whole circuit can be outgassed using a vacuum pump. Then, the upstream and downstream reservoirs are filled with the gas mixture from a high pressure tank. The pressure level is independently controlled in each reservoir with a pressure regulator. As soon as the waiting until thermal equilibrium is reached, valves are opened allowing the gas flow from the upstream to the downstream reservoir, through the microsystem. During the measure, upstream and downstream pressures are submitted to a small (typically 1–2%) decrease and increase, respectively. The temperature in the experiments is 298.5 K, and during operation, the temperature variation is measured with four PT100 temperature sensors (with a 0.15 K accuracy). Based on these measurements, the temperature standard deviation during each experiment is less than 0.1 K. Most of the setup is made of stainless steel, aluminum, or glass, and the connections are insured by ISO-KF and Swagelok Ultra-Torr® components to avoid any leakage during low pressure operation. Air tightness has been checked by means of helium detection, with a portable high precision leak detector.

From the measurement of the pressure variation in each reservoir, two experimental values of the molar flow rate can be deduced from

$$J_A^{\mathrm{e}} = -\frac{\mathrm{d}N_A}{\mathrm{d}t} = -\frac{V_A}{R_{\mathrm{g}}}\frac{\mathrm{d}}{\mathrm{d}t}\left(\frac{P_A}{T_A}\right), \quad J_B^{\mathrm{e}} = \frac{\mathrm{d}N_B}{\mathrm{d}t} = \frac{V_B}{R_g}\frac{\mathrm{d}}{\mathrm{d}t}\left(\frac{P_B}{T_B}\right), \tag{19}$$

where $t$ is the time, $N_A$ and $N_B$ are the amounts of gas molecules in mol units in the upstream and downstream reservoirs, respectively. $P_A$ and $T_A$, $P_B$ and $T_B$ are the pressures and temperatures in these reservoirs of respective volumes $V_A$ and $V_B$, and $R_{\mathrm{g}} = k \times (6.022 \times 10^{23}/\mathrm{mol})$ is the global gas constant. The experimental molar flow rate leaving the upstream reservoir is compared with the experimental molar flow rate entering the downstream reservoir. It is verified that deviation between the two values is well within the experimental uncertainty, and the average experimental molar flow rate can be defined as

$$J^{\mathrm{e}} = \frac{J_A^{\mathrm{e}} + J_B^{\mathrm{e}}}{2}. \tag{20}$$

At this point, a discussion on the definition of the molar and mass flow rates is needed. In experiments with single component gases, the mass flow rate $\mathrm{d}M/\mathrm{d}t$, instead of the molar flow rate $\mathrm{d}N/\mathrm{d}t$, is commonly introduced. Since, in general, $M = N \times m^*$, with $m^*$ denoting the average molecular mass of the particles flowing through the channel during the experiment, the mass flow rate is obtained from Eq. 19 as

$$\frac{\mathrm{d}M}{\mathrm{d}t} = \pm\frac{V}{RT}\frac{\mathrm{d}P}{\mathrm{d}t}, \tag{21}$$

where, $R = k/m^*$ is the specific gas constant. For single component gases, the average mass $m^*$ is equal to the molecular mass. However, for gaseous mixtures, $m^*$ cannot be defined, since it refers to that gas portion which has flowed through the channel during the experiment. Because of the diffusion effects, that is the lighter particle has larger velocity than the heavier one, the concentration of this gas portion, denoted by $C^*$, is different from the concentrations in the two reservoirs ($C_A$ and $C_B$), and it is not determined. In fact, this concentration can be expressed as $C^* = J_1/(J_1 + J_2)$, and then the average mass is obtained by $m^* = C^* m_1 + (1 - C^*)m_2$. However, the component fluxes, $J_1$ and $J_2$ and consequently $m^*$, cannot be determined from the present experimental approach. They are estimated only from the computational approach. Therefore, the experimental results and the comparative study are based on the molar and not on the mass flow rates.

Following from Eq. 19, the total molar flow rate through the channel is expressed by

$$\begin{aligned} J_A^{\mathrm{e}} &= -\frac{\mathrm{d}N_A}{\mathrm{d}t} = -\frac{V_A}{R_{\mathrm{g}}T_A}\frac{\mathrm{d}P_A}{\mathrm{d}t}\left(1 - \frac{\mathrm{d}T_A/T_A}{\mathrm{d}P_A/P_A}\right), \\ J_B^{\mathrm{e}} &= \frac{\mathrm{d}N_B}{\mathrm{d}t} = \frac{V_B}{R_{\mathrm{g}}T_B}\frac{\mathrm{d}P_B}{\mathrm{d}t}\left(1 - \frac{\mathrm{d}T_B/T_B}{\mathrm{d}P_B/P_B}\right). \end{aligned} \tag{22}$$

As mentioned above, high-thermal stability is ensured by two temperature-regulation systems. The relative temperature variation $\mathrm{d}T/T$ is then, of the order of $4 \times 10^{-4}$, to be compared with the relative pressure variation $\mathrm{d}P/P \approx 2 \times 10^{-2}$. As a consequence, Eq. 22 can be written as

$$J_A^{\mathrm{e}} = -\frac{V_A}{R_{\mathrm{g}}T_A}a_A c_A, \quad J_B^{\mathrm{e}} = \frac{V_B}{R_{\mathrm{g}}T_B}a_B c_B, \tag{23}$$

where $a = \mathrm{d}P/\mathrm{d}t$ is calculated from a least-square linear fit of the upstream or downstream measured pressure

$$P_A(t) = a_A t + b_A, \quad J_B^{\mathrm{e}} = a_B t + b_B, \tag{24}$$

and $c = 1 - (\mathrm{d}T/T)/(\mathrm{d}P/P) = 1 \pm 2\%$. More than 1000 pressure data are used for determining coefficients $a$ and $b$. The standard deviation of coefficient $a$ is calculated following the method proposed in Pitakarnnop et al. (2010) and is found to be less than 0.5%. Therefore, the overall uncertainty of the molar flow rate measurement is calculated from

$$\frac{\Delta J_A^e}{J_A^e} = \frac{\Delta J_B^e}{J_B^e} = \frac{\Delta V}{V} + \frac{\Delta T}{T} + \frac{\Delta a}{a} + \frac{\Delta c}{c}, \quad (25)$$

and is less than $\pm(1.3 + 0.2 + 0.5 + 2)\% = \pm 4\%$.

Finally, it should be noted that outgassing from the setup when operating at low pressure could generally not be neglected, and, consequently, must be measured. In that case, a three-step procedure is used:

1. Outgassing is first quantified in the downstream circuit B, including reservoir B and all connections up to the microsystem outlet. In order to avoid flow through the microsystem during this operation, both upstream and downstream circuits are pressurized to the downstream operating pressure, and the valve placed between circuit A and the microchannel is closed. As soon as thermal stability is reached, the pressure rise in circuit B, which now is only due to outgassing, is measured.
2. After this step, pressure in the upstream circuit A is increased up to the desired upstream value and once thermal stability is reached, the pressure variations in circuits A and B are measured during the flow of the gas mixture from circuit A to circuit B through the microsystem.
3. Finally, outgassing is quantified in circuit A, including all connections up to the microsystem inlet. For this purpose, pressure in circuit B is increased to the same level as in circuit A, to avoid flow through the microsystem due to a pressure gradient, and the valve between circuit B and the microsystem is closed; then, the pressure rise in circuit A is monitored.

Outgassing rates in each circuit are calculated using Eqs. 23 and 24 and used to correct the flow rate data. The uncertainties shown in Eq. 25 are also taken into account for the calculation of the outgassed flow rate, and the total uncertainty represented by vertical bars in Figs. 1, 2, and 3 takes into account all uncertainties introduced in the three steps of the operating procedure. As a consequence, when outgassing is not negligible, the total uncertainty is given by

$$\frac{\Delta J_A^e}{J_A^e} = \pm 0.04\left(1 + 2\frac{J_{ogA}^e}{J_A^e}\right), \quad \frac{\Delta J_B^e}{J_B^e} = \pm 0.04\left(1 + 2\frac{J_{ogB}^e}{J_B^e}\right), \quad (26)$$

where $J_{ogA}^e$ is the molar flow rate due to outgassing in circuit A calculated from the third step of the procedure, and $J_{ogB}^e$ is the molar flow rate due to outgassing in circuit B calculated from the first step of the procedure. The coefficient 2 in the brackets of the right-hand side terms of Eq. 26 is due to the fact that outgassing occurs in steps 2 and 3 (respectively 1 and 2) necessary for calculating $J_A^e$ (respectively $J_B^e$). It should be outlined that outgassing is essentially due to the manufactured parts of circuits A and B, although outgassing from the walls of the microchannels can be neglected, first because silicon and glass wafers have very clean surfaces and second because the surface area of the microchannels walls is typically ten orders of magnitude lower than the total surface area of circuits A or B.

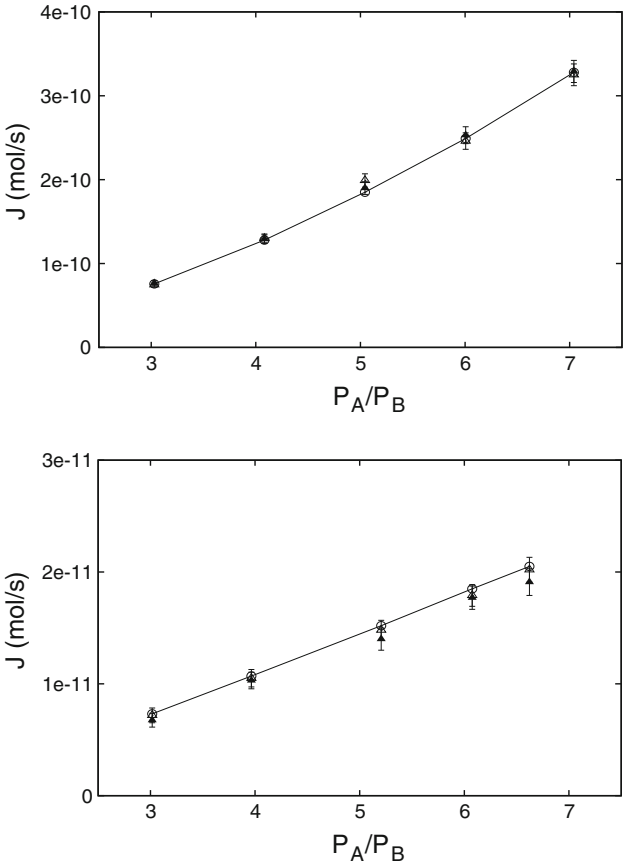


**Fig. 1** Computational and experimental total molar flow rates of He–Ar ($C_A = 0.1017$), with (i) $P_B \approx 15$ kPa (*up*) and (ii) $P_B \approx 2$ kPa (*down*). The symbols *circle*, *open triangle*, and *filled triangle* represent $J$, $J_A^e$, and $J_B^e$, respectively. The *solid line* is plotted to guide the eyes for the computational results of $J$

Finally, the comparison of the upstream and downstream resulting flow rates $J_A^e$ and $J_B^e$ is an indirect mean for verifying that the outgassing effects are well taken into account by the procedure described above, whatever the level of outgassing.

## 5 Results

Computational and experimental results in tabulated and graphical form are provided for the flow of the He–Ar gaseous mixture through the microsystem consisting of a series of 45 identical rectangular microchannels. The reference concentration $C_A$ of the gas mixture, which as

defined before, refers to the concentration of He in the mixture varies between zero and one, taking the following values: $C_A = [0.0, 0.1017, 0.3012, 0.5010, 0.7019, 0.9014, 1.0]$. These values cover the whole range of the concentration interval from pure Ar ($C_A = 0$) to pure He ($C_A = 1$). For these values of exact concentration, the corresponding uncertainties are [0, ±0.002, ±0.006, ±0.010, ±0.006, ±0.002, 0], respectively. The effect of the concentration uncertainty on the numerical calculations has been verified, and it was found that the introduced uncertainty for the flow rates is less than ±0.5%. Two values of downstream pressure $P_B$, namely, $P_B \approx 15$ kPa and $P_B \approx 2$ kPa, are considered. In both cases, the upstream to downstream pressure ratio varies approximately from three to seven. Therefore, the results are presented into two groups depending on $P_B$. The average Knudsen number varies in the first group with $P_B \approx 15$ kPa, as $0.1 < Kn_0 < 0.6$, and in the second group with $P_B \approx 2$ kPa, as $1.0 < Kn_0 < 4.0$. It is seen that the largest portion of the transition regime is covered. Results in the slip regime may be found in Pitakarnnop et al. (2010).

Based on the above flow parameters, Tables 1 and 2 present computational and experimental flow rates for $P_B \approx 15$ kPa and $P_B \approx 2$ kPa, respectively. In these tables, the first three columns provide the values of the reference concentration $C_A$, the pressure ratio $P_A/P_B$, and

**Table 1** Computational and experimental molar flow rates of He–Ar for various concentrations $C_A$ and pressure ratios $P_A/P_B$, with $P_B \approx 15$ kPa

| $C_A$ | $P_A/P_B$ | $Kn_0$ | $J_1$ (mol/s) | $J_2$ (mol/s) | $J$ (mol/s) | $J^e$ (mol/s) | Δ |
|---|---|---|---|---|---|---|---|
| 0.0 | 3.06 | 0.175 | 0.00 | 7.57 (−11) | 7.57 (−11) | 7.28 (−11) | 3.97 |
| | 4.06 | 0.165 | 0.00 | 1.26 (−10) | 1.26 (−10) | 1.21 (−10) | 3.62 |
| | 5.06 | 0.159 | 0.00 | 1.86 (−10) | 1.86 (−10) | 1.79 (−10) | 3.40 |
| | 6.01 | 0.154 | 0.00 | 2.51 (−10) | 2.51 (−10) | 2.43 (−10) | 3.45 |
| | 7.00 | 0.151 | 0.00 | 3.28 (−10) | 3.28 (−10) | 3.13 (−10) | 4.90 |
| 0.1017 | 3.03 | 0.197 | 8.80 (−12) | 6.70 (−11) | 7.58 (−11) | 7.56 (−11) | 0.23 |
| | 4.08 | 0.184 | 1.42 (−11) | 1.14 (−10) | 1.29 (−10) | 1.29 (−10) | −0.77 |
| | 5.04 | 0.178 | 1.99 (−11) | 1.65 (−10) | 1.85 (−10) | 1.94 (−10) | −4.79 |
| | 6.01 | 0.173 | 2.64 (−11) | 2.23 (−10) | 2.50 (−10) | 2.49 (−10) | 0.15 |
| | 7.04 | 0.169 | 3.44 (−11) | 2.94 (−10) | 3.28 (−10) | 3.26 (−10) | 0.50 |
| 0.3012 | 3.04 | 0.225 | 2.85 (−11) | 5.62 (−11) | 8.48 (−11) | 8.38 (−11) | 1.16 |
| | 4.02 | 0.212 | 4.39 (−11) | 9.20 (−11) | 1.36 (−10) | 1.36 (−10) | 0.19 |
| | 5.03 | 0.203 | 6.27 (−11) | 1.35 (−10) | 1.98 (−10) | 2.00 (−10) | −0.80 |
| | 6.04 | 0.197 | 8.37 (−11) | 1.84 (−10) | 2.68 (−10) | 2.70 (−10) | −0.50 |
| | 7.00 | 0.194 | 1.06 (−10) | 2.37 (−10) | 3.43 (−10) | 3.42 (−10) | 0.24 |
| 0.5010 | 3.10 | 0.262 | 5.40 (−11) | 4.54 (−11) | 9.93 (−11) | 9.80 (−11) | 1.38 |
| | 4.09 | 0.246 | 8.28 (−11) | 7.42 (−11) | 1.57 (−10) | 1.59 (−10) | −1.03 |
| | 5.05 | 0.237 | 1.14 (−10) | 1.05 (−10) | 2.20 (−10) | 2.16 (−10) | 1.41 |
| | 6.02 | 0.231 | 1.51 (−10) | 1.41 (−10) | 2.92 (−10) | 2.90 (−10) | 0.48 |
| | 7.00 | 0.226 | 1.91 (−10) | 1.82 (−10) | 3.73 (−10) | 3.73 (−10) | −0.18 |
| 0.7019 | 3.05 | 0.309 | 8.49 (−11) | 3.02 (−11) | 1.15 (−10) | 1.07 (−10) | 7.24 |
| | 4.03 | 0.291 | 1.31 (−10) | 4.91 (−11) | 1.80 (−10) | 1.73 (−10) | 4.15 |
| | 5.02 | 0.280 | 1.82 (−10) | 7.11 (−11) | 2.53 (−10) | 2.39 (−10) | 5.69 |
| | 5.98 | 0.272 | 2.38 (−10) | 9.45 (−11) | 3.32 (−10) | 3.15 (−10) | 5.60 |
| | 7.01 | 0.267 | 3.03 (−10) | 1.22 (−10) | 4.25 (−10) | 4.09 (−10) | 3.96 |
| 0.9014 | 2.99 | 0.402 | 1.28 (−10) | 1.16 (−11) | 1.40 (−10) | 1.38 (−10) | 1.24 |
| | 4.04 | 0.376 | 2.05 (−10) | 1.97 (−11) | 2.24 (−10) | 2.23 (−10) | 0.80 |
| | 5.03 | 0.361 | 2.85 (−10) | 2.83 (−11) | 3.13 (−10) | 3.11 (−10) | 0.57 |
| | 6.09 | 0.351 | 3.79 (−10) | 3.87 (−11) | 4.18 (−10) | 4.17 (−10) | 0.04 |
| | 6.96 | 0.345 | 4.63 (−10) | 4.78 (−11) | 5.11 (−10) | 5.09 (−10) | 0.46 |
| 1.0 | 3.03 | 0.511 | 1.65 (−10) | 0.00 | 1.65 (−10) | 1.68 (−10) | −2.15 |
| | 4.00 | 0.481 | 2.55 (−10) | 0.00 | 2.55 (−10) | 2.57 (−10) | −0.94 |
| | 5.01 | 0.461 | 3.58 (−10) | 0.00 | 3.58 (−10) | 3.65 (−10) | −1.90 |
| | 6.01 | 0.449 | 4.70 (−10) | 0.00 | 4.70 (−10) | 4.77 (−10) | −1.42 |
| | 6.94 | 0.440 | 5.83 (−10) | 0.00 | 5.83 (−10) | 6.00 (−10) | −2.74 |

the resulting average Knudsen number $Kn_0$, respectively. For each concentration examined, five different pressure ratios are considered. The fourth and fifth columns provide the computational results of the molar flow rates of each species, $J_1$ and $J_2$, followed in the sixth column with the total computational flow rate $J = J_1 + J_2$. The flow rates are presented in a normalized floating-point form. All values are given with an accuracy of three significant figures, and the exponents with base 10 are provided in parenthesis. This notation is common in rarefied gas calculations. The experimental total molar flow rates, denoted by $J^e$ are given in the seventh column, while in the last column of both tables (column 8 in Table 1 and column 10 in Table 2), the relative deviation between $J$ and $J^e$, defined as $\Delta = 100(J/J^e - 1)$, is shown. Finally, the total experimental uncertainties are provided. The uncertainty for the experimental molar flow rates in Table 1 with $P_B \approx 15$ kPa, where outgassing is negligible, is in all cases $\pm 4\%$. However, the uncertainties for the results in Table 2 with $P_B \approx 2$ kPa, where outgassing is not negligible, is case dependent. In this latter situation, the uncertainties for the inlet and outlet flow rates, denoted by $\Delta J_A^e$ and $\Delta J_B^e$, are given in percentages in the eighth and ninth columns of Table 2.

**Table 2** Computational and experimental molar flow rates of He–Ar for various concentrations $C_A$ and pressure ratios $P_A/P_B$, with $P_B \approx 2$ kPa

| $C_A$ | $P_A/P_B$ | $Kn_0$ | $J_1$ (mol/s) | $J_2$ (mol/s) | $J$ (mol/s) | $J^e$ (mol/s) | $\Delta J_A^e$ | $\Delta J_B^e$ | $\Delta$ |
|---|---|---|---|---|---|---|---|---|---|
| 0.0 | 3.10 | 1.31 | 0.00 | 6.56 (−12) | 6.56 (−12) | 6.51 (−12) | 9.67 | 9.58 | 0.82 |
| | 4.02 | 1.26 | 0.00 | 9.31 (−12) | 9.31 (−12) | 8.86 (−12) | 8.59 | 8.56 | 5.02 |
| | 4.79 | 1.18 | 0.00 | 1.22 (−11) | 1.22 (−11) | 1.20 (−11) | 7.30 | 7.76 | 1.93 |
| | 5.96 | 1.17 | 0.00 | 1.59 (−11) | 1.59 (−11) | 1.51 (−11) | 6.84 | 7.50 | 4.97 |
| | 6.61 | 1.11 | 0.00 | 1.89 (−11) | 1.89 (−11) | 1.83 (−11) | 6.03 | 6.55 | 3.08 |
| 0.1017 | 3.02 | 1.48 | 1.47 (−12) | 5.85 (−12) | 7.32 (−12) | 6.96 (−12) | 9.24 | 9.14 | 5.20 |
| | 3.96 | 1.39 | 2.05 (−12) | 8.68 (−12) | 1.07 (−11) | 1.03 (−11) | 7.42 | 7.22 | 3.65 |
| | 5.21 | 1.32 | 2.73 (−12) | 1.25 (−11) | 1.52 (−11) | 1.44 (−11) | 5.95 | 7.09 | 5.88 |
| | 6.08 | 1.29 | 3.18 (−12) | 1.53 (−11) | 1.85 (−11) | 1.78 (−11) | 5.40 | 5.88 | 3.93 |
| | 6.62 | 1.28 | 3.44 (−12) | 1.71 (−11) | 2.05 (−11) | 1.97 (−11) | 5.50 | 6.25 | 4.33 |
| 0.3012 | 3.07 | 1.68 | 4.76 (−12) | 5.00 (−12) | 9.76 (−12) | 8.82 (−12) | 7.90 | 8.33 | 10.6 |
| | 4.03 | 1.58 | 6.67 (−12) | 7.44 (−12) | 1.41 (−11) | 1.27 (−11) | 6.44 | 6.95 | 10.8 |
| | 5.00 | 1.52 | 8.43 (−12) | 9.98 (−12) | 1.84 (−11) | 1.75 (−11) | 5.75 | 5.60 | 5.34 |
| | 5.94 | 1.50 | 9.94 (−12) | 1.24 (−11) | 2.23 (−11) | 2.12 (−11) | 5.39 | 5.53 | 5.30 |
| | 6.67 | 1.45 | 1.13 (−11) | 1.47 (−11) | 2.60 (−11) | 2.40 (−11) | 5.19 | 5.83 | 8.17 |
| 0.5010 | 3.03 | 1.97 | 8.38 (−12) | 3.78 (−12) | 1.22 (−11) | 1.13 (−11) | 6.12 | 6.35 | 7.11 |
| | 4.06 | 1.85 | 1.21 (−11) | 5.80 (−12) | 1.79 (−11) | 1.66 (−11) | 5.20 | 5.66 | 7.45 |
| | 5.03 | 1.78 | 1.54 (−11) | 7.81 (−12) | 2.32 (−11) | 2.11 (−11) | 4.80 | 5.27 | 9.76 |
| | 5.91 | 1.73 | 1.82 (−11) | 9.72 (−12) | 2.79 (−11) | 2.54 (−11) | 4.67 | 5.11 | 10.06 |
| | 6.42 | 1.71 | 1.98 (−11) | 1.09 (−11) | 3.07 (−11) | 2.83 (−11) | 4.71 | 4.92 | 8.23 |
| 0.7019 | 3.06 | 2.32 | 1.29 (−11) | 2.50 (−12) | 1.54 (−11) | 1.41 (−11) | 5.63 | 5.78 | 9.22 |
| | 3.94 | 2.20 | 1.78 (−11) | 3.67 (−12) | 2.15 (−11) | 2.00 (−11) | 4.92 | 5.22 | 7.05 |
| | 5.42 | 2.07 | 2.58 (−11) | 5.77 (−12) | 3.16 (−11) | 2.90 (−11) | 4.59 | 4.95 | 8.92 |
| | 5.87 | 2.05 | 2.81 (−11) | 6.43 (−12) | 3.46 (−11) | 3.13 (−11) | 4.50 | 4.89 | 10.6 |
| | 6.33 | 2.03 | 3.05 (−11) | 7.15 (−12) | 3.77 (−11) | 3.41 (−11) | 4.46 | 4.83 | 10.4 |
| 0.9014 | 3.01 | 3.01 | 1.78 (−11) | 8.97 (−13) | 1.87 (−11) | 1.80 (−11) | 5.47 | 5.53 | 3.63 |
| | 3.95 | 2.83 | 2.56 (−11) | 1.37 (−12) | 2.70 (−11) | 2.60 (−11) | 4.86 | 5.05 | 3.79 |
| | 5.20 | 2.70 | 3.56 (−11) | 2.06 (−12) | 3.77 (−11) | 3.56 (−11) | 4.66 | 5.18 | 5.77 |
| | 5.88 | 2.64 | 4.11 (−11) | 2.46 (−12) | 4.35 (−11) | 4.08 (−11) | 4.43 | 4.74 | 6.67 |
| | 6.31 | 2.62 | 4.45 (−11) | 2.71 (−12) | 4.72 (−11) | 4.53 (−11) | 4.27 | 4.61 | 4.11 |
| 1.0 | 3.12 | 3.95 | 2.12 (−11) | 0.00 | 2.12 (−11) | 1.95 (−11) | 6.63 | 6.44 | 9.04 |
| | 3.92 | 3.61 | 2.99 (−11) | 0.00 | 2.99 (−11) | 2.77 (−11) | 5.58 | 5.96 | 7.81 |
| | 4.97 | 3.44 | 4.04 (−11) | 0.00 | 4.04 (−11) | 3.82 (−11) | 5.05 | 5.34 | 5.69 |
| | 5.83 | 3.40 | 4.83 (−11) | 0.00 | 4.83 (−11) | 4.62 (−11) | 4.83 | 5.02 | 4.41 |
| | 6.81 | 3.34 | 5.76 (−11) | 0.00 | 5.76 (−11) | 5.45 (−11) | 4.52 | 4.92 | 5.74 |

Comparing the quantities in Table 1 with those in Table 2, it is seen that in Table 1, the average Knudsen numbers and flow rates are about one order of magnitude smaller than the ones in Table 2. The deviation $\Delta$ in Table 1 varies between $-4.79$ and 7.24% with an average value of 1.07%, while in Table 2 it is between 0.82 and 10.8% with the average value equal to 6.41%. It is seen that in the latter case the experimental results are always less than the corresponding computational ones. Also, in general, the deviations $\Delta$ in Table 1 are much smaller than the corresponding ones in Table 2.

A complementary picture on the comparison between computational and experimental results, may be obtained by examining Figs. 1, 2, and 3, where results are provided for $C_A = 0.1017$, 0.5010, and 0.9014, respectively. In these figures in addition to the computational total flow rates $J$, the corresponding experimental ones at the inlet and outlet reservoirs $J_A^e$ and $J_B^e$, respectively, with their associated bars of uncertainty are presented. It is clearly observed that in all cases the agreement between the results is much better for $P_B \approx 15$ kPa rather than for $P_B \approx 2$ kPa. In particular,

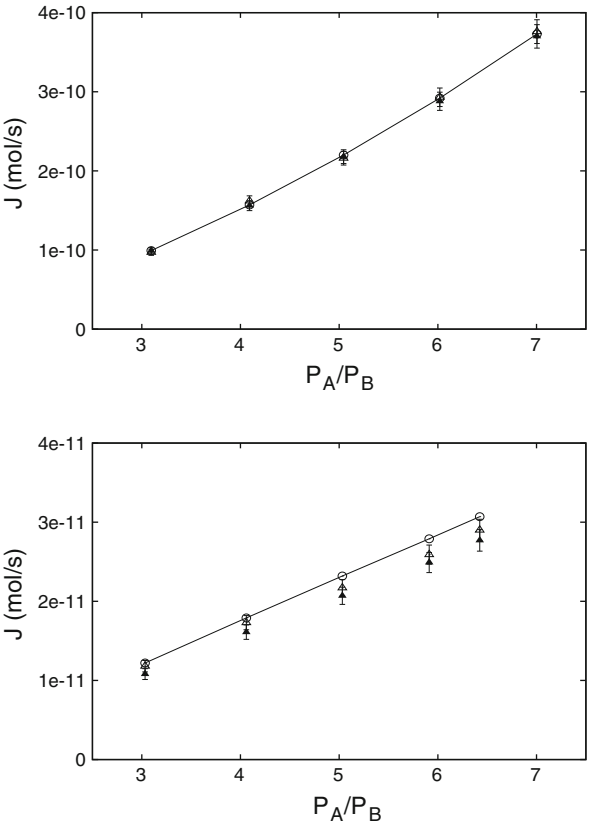


**Fig. 2** Computational and experimental total molar flow rates of He–Ar ($C_A = 0.5010$), with (i) $P_B \approx 15$ kPa (*up*) and (ii) $P_B \approx 2$ kPa (*down*). The symbols *open circle*, *open triangle*, and *filled triangle* represent $J$, $J_A^e$, and $J_B^e$, respectively. The *solid line* is plotted to guide the eyes for the computational results of $J$

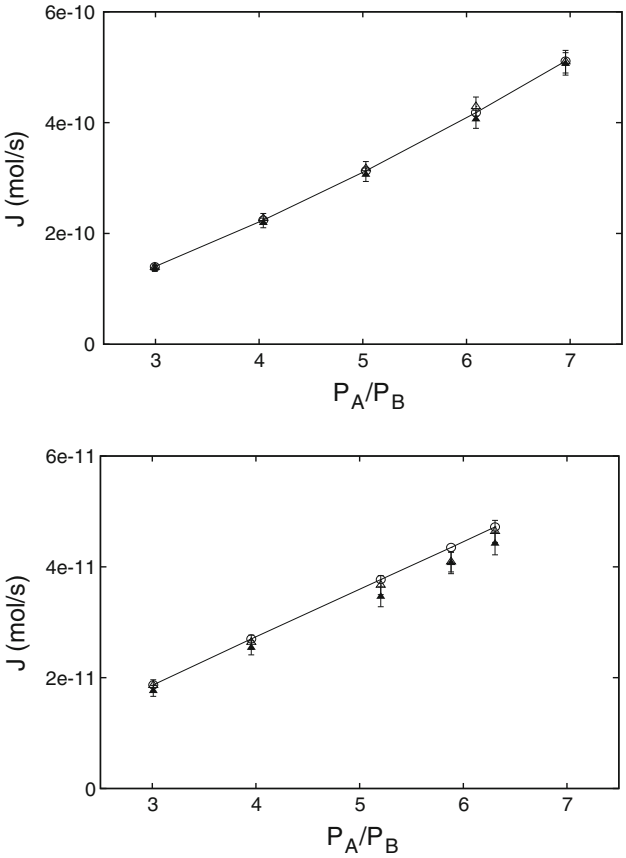


**Fig. 3** Computational and experimental total molar flow rates of He–Ar ($C_A = 0.9014$), with (i) $P_B \approx 15$ kPa (*up*) and (ii) $P_B \approx 2$ kPa (*down*). The symbols *open circle*, *open triangle*, and *filled triangle* represent $J$, $J_A^e$, and $J_B^e$, respectively. The *solid line* is plotted to guide the eyes for the computational results of $J$

for $P_B \approx 15$ kPa, the computational results are always well within the dispersion range of the experimental results, while for $P_B \approx 2$ kPa, in some cases, they are within the experimental uncertainties and, in other cases, they are at the upper margin of the experimental dispersion bars. This behavior is attributed to the fact that both experimental uncertainties and kinetic modeling errors are increased as the gas rarefaction is increased. In particular, based on the above discussion, it is clear that the experimental uncertainties, mainly due to outgassing, are reduced in the case of higher downstream pressure $P_B \approx 15$ kPa. Also, in this case, since the gas is more dense, the flow lies in the slip or early transition region, and the McCormack model description provides a more accurate description of the transport coefficients and the flow field. In the case of lower downstream pressure $P_B \approx 2$ kPa, the gas is more dilute and the increased rarefaction may introduce some mismatch between the McCormack model and the true experimental results. However, the overall deviation between computational and experimental results is within

the introduced modeling and measurement uncertainties and, therefore, it is considered as very good.

As mentioned before, the computational approach in addition to the molar flow rates yields the pressure and concentration distributions along the channel. Some typical results of the axial distributions $P(z'/L)/P_B$ and $C(z'/L)$ are shown in Figs. 4 and 5 for $P_B \approx 15$ kPa and $P_B \approx 2$ kPa, respectively. These data correspond to the case of $C_A = 0.5$ in Table 1, with each plot in the figures corresponding to a given pressure ratio. The inlet and outlet values are, for the pressure distribution $P(0) = P_A/P_B$ and $P(1) = 1$ and for the concentration distribution $C(0) = C(1) = 0.5$. The pressure distributions have a qualitative behavior, which is similar to the one observed in pressure-driven single gas flow configurations (Varoutis et al. 2009). They are linear in highly rarefied atmospheres, and then they are gradually converted to nonlinear as the atmosphere becomes less rarefied. Next, turning to the concentration distributions, it is clearly seen that they are non-uniform along the channel. Both in Figs. 4 and 5, starting from the

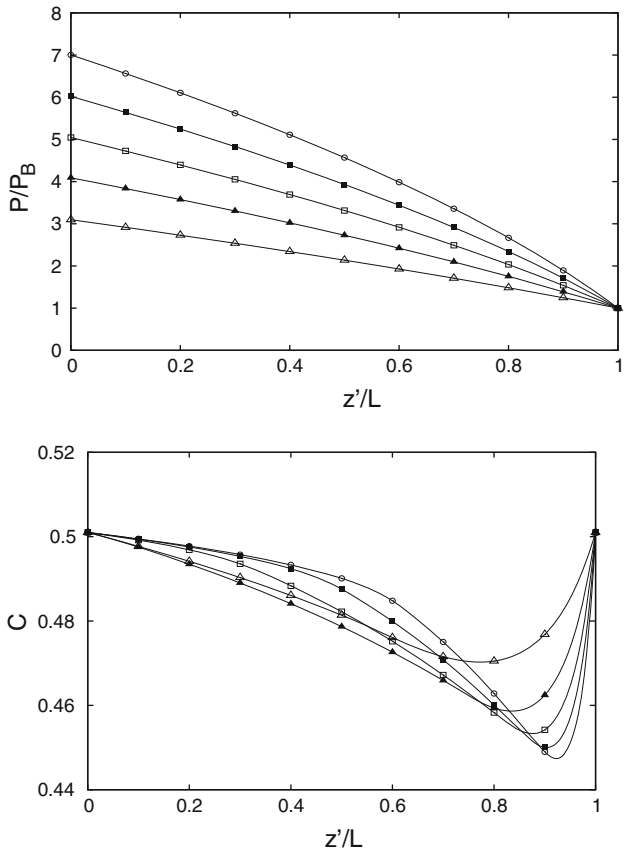


**Fig. 4** Distributions of normalized pressure (*up*) and concentration (*down*) for He–Ar ($C_A = 0.5010$) along the channel, with $P_B \approx 15$ kPa. The symbols *open triangle*, *filled triangle*, *open square*, *filled square*, and *open circle* correspond to results for $P_A/P_B = [3.01, 4.09, 5.04, 6.02, \text{and } 7.00]$, respectively

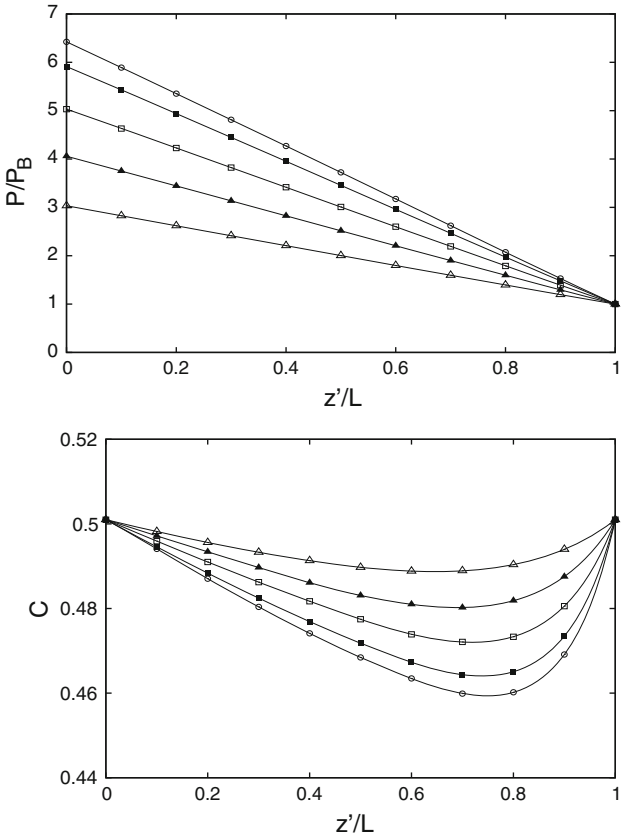


**Fig. 5** Distributions of normalized pressure (*up*) and concentration (*down*) for He–Ar ($C_A = 0.5010$) along the channel, with $P_B \approx 2$ kPa. The symbols *open triangle*, *filled triangle*, *open square*, *filled square*, and *open circle* correspond to results for $P_A/P_B = [3.03, 4.06, 5.03, 5.91, \text{and } 6.42]$, respectively

inlet point, the concentration decreases, taking its minimum value of $C \approx 0.45$ somewhere at the second half of the channel, and then it increases and reaches the outlet value. The point in the channel where the minimum value occurs is different for each pressure ratio and downstream pressure. Also, the qualitative behavior between the concentration distributions for $P_B \approx 15$ kPa and $P_B \approx 2$ kPa is different, with the latter ones having a more smooth variation along the channel. The deviation of the concentration from the uniform distribution is larger for the case $P_B \approx 2$ kPa. In this situation, the gas is more dilute and the diffusion effects are more important resulting into the increased separation of the gaseous components.

## 6 Concluding remarks

The pressure-driven binary gas flow through a rectangular microchannel has been investigated both computationally and experimentally. The computational approach is based on the numerical solution of the McCormack kinetic model

and the experimental approach on the Constant Volume method. Based on the computed and measured total molar flow rates, a systematic and detailed comparison has been performed finding very good agreement in a wide range of the Knudsen numbers inside the transition regime. This outcome clearly demonstrates that the McCormack model and the associated numeric scheme can be successfully implemented to simulate pressure-driven microflows of gaseous mixtures, providing accurate results with modest computational effort. This remark is important taking into account the feasibility of the theoretical–computational scheme to easily provide solutions to other micro-flow configurations and its potential to investigate complex non-equilibrium phenomena such as diffusion effects.

**Acknowledgment** The research leading to these results has received funding from the European Community's Seventh Framework Programme (FP7/2007-2013) under grant agreement no 215504.

## References

Aoki K (2001) Dynamics of rarefied gas flows: asymptotic and numerical analyses of the Boltzmann equation. In: 39th AIAA aerospace science meeting and exhibit, Reno, 2001-0874

Bird GA (1994) Molecular gas dynamics and the direct simulation of gas flows. Oxford University Press, Oxford

Breyiannis G, Varoutis S, Valougeorgis D (2008) Rarefied gas flow in concentric annular tube: estimation of the Poiseuille number and the exact hydraulic diameter. Eur J Mech B Fluids 27:609–622

Cercignani C (1988) The Boltzmann equation and its application. Springer-Verlag, New York

Colin S (2005) Rarefaction and compressibility effects on steady and transient gas flows in microchannels. Microfluid Nanofluidics 1:268–279

Colin S, Lalonde P, Caen R (2004) Validation of a second-order slip flow model in rectangular microchannels. Heat Transf Eng 25:23–30

De Groot SR, Mazut P (1984) Non-equilibrium thermodynamics. Dover, New York

Ewart T, Perrier P, Graur I, Méolans JG (2006) Mass flow rate measurements in gas micro flow. Exp Fluids 41:487–498

Ewart T, Perrier P, Graur IA, Méolans JG (2007) Mass flow rate measurements in a microchannel, from hydrodynamic to near free molecular regimes. J Fluid Mech 584:337–356

Ferziger JH, Kaper HG (1972) Mathematical theory of transport processes in gases. North Holland, Amsterdam

Harley JC, Huang Y, Bau HH, Zemel JN (1995) Gas flow in micro-channels. J Fluid Mech 284:257–274

Ho CM, Tai YC (1998) Micro-electro-mechanical-systems (MEMS) and fluid flows. Annu Rev Fluid Mech 30:579–612

Ivchenko IN, Loyalka SK, Tompson RV (1997) Slip coefficients for binary gas mixture. J Vac Sci Technol A 15:2375–2381

Kandlikar SG, Garimella S, Li D, Colin S, King MR (2006) Heat transfer and fluid flow in minichannels and microchannels. Elsevier, Oxford

Kestin J, Knierim K, Mason EA, NajaB B, Ro ST, Waldman M (1984) Equilibrium and transport properties of the noble gases and their mixture at low densities. J Phys Chem Ref Data 13:229–303

Kosuge S, Takata S (2008) Database for flows of binary mixtures through a plane microchannel. Eur J Mech B Fluids 27:444–465

Lockerby DA, Reese JM (2008) On the modelling of isothermal gas flows at the microscale. J Fluid Mech 604:235–261

Marino L (2009) Experiments on rarefied gas flows through tubes. Microfluid Nanofluidics 6:109–119

Maurer J, Tabeling P, Joseph P, Willaime H (2003) Second-order slip laws in microchannels for helium and nitrogen. Phys Fluids 15:2613–2621

McCormack FJ (1973) Construction of linearized kinetic models for gaseous mixtures and molecular gases. Phys Fluids 16:2095–2105

Morini GL, Lorenzini M, Spiga M (2005) A criterion for experimental validation of slip-flow models for incompressible rarefied gases through microchannels. Microfluid Nanofluidics 1:190–196

Naris S, Valougeorgis D, Kalempa D, Sharipov F (2004a) Discrete velocity modelling of gaseous mixture flows in MEMS. Superlattices Microstruct 35:629-643

Naris S, Valougeorgis D, Kalempa D, Sharipov F (2004b) Gaseous mixture flow between two parallel plates in the whole range of the gas rarefaction. Physica A 336:294–318

Naris S, Valougeorgis D, Kalempa D, Sharipov F (2005) Flow of gaseous mixtures through rectangular microchannels driven by pressure, temperature and concentration gradients. Phys Fluids 17:100607.1–100607.12

Pitakarnnop J (2009) Analyse expérimentale et simulation numérique d'écoulements raréfiés de gaz simples et de mélanges gazeux dans les microcanaux. Ph.D. thesis, University of Toulouse

Pitakarnnop J, Geoffroy S, Colin S, Baldas L (2008) Slip flow in triangular and trapezoidal microchannels. Int J Heat Technol 26:167–174

Pitakarnnop J, Varoutis S, Valougeorgis D, Geoffroy S, Baldas L, Colin S (2010) A novel experimental setup for gas microflows. Microfluid Nanofluidics 8:57–72

Sharipov F (1994) Onsager-Casimir reciprocity relations for open gaseous systems at arbitrary rarefaction III. Theory and its application for gaseous mixtures. Physica A 209:457–476

Sharipov F (1999) Rarefied gas flow through a long rectangular channel. J Vac Sci Technol A 17:3062–3066

Sharipov F, Seleznev V (1998) Data on internal rarefied gas flows. J Phys Chem Ref Data 27:657–706

Sharipov F, Kalempa D (2002) Gaseous mixture flow through a long tube at arbitrary Knudsen number. J Vac Sci Technol A 20:814–822

Sharipov F, Kalempa D (2003) Velocity slip and temperature jump coefficients for gaseous mixtures. I. Viscous slip problem. Phys Fluids 15:1800–1806

Sharipov F, Kalempa D (2005) Separation phenomena for gaseous mixture flowing through a long tube into vacuum. Phys Fluids 17:127102.1–127102.8

Siewert CE, Valougeorgis D (2004) The McCormack model: channel flow of a binary gas mixture driven by temperature, pressure and density gradients. Eur J Mech B Fluids 23:645–664

Szalmas L (2007) Multiple-relaxation time lattice Boltzmann method for the finite Knudsen number region. Physica A 379:401–408

Szalmas L, Valougeorgis D (2010) Rarefied gas flow of binary mixtures through long channels with triangular and trapezoidal cross sections. Microfluid Nanofluidics. doi:10.1007/s10404-010-0564-9

Takata S, Yasuda S, Kosuge S, Aoki K (2003) Numerical analysis of thermal-slip and diffusion-slip flows of a binary mixture of hard-sphere molecular gases. Phys Fluids 15:3745-3766

Takata S, Sugimoto H, Kosuge S (2007) Gas separation by means of the Knudsen compressor. Eur J Mech B Fluids 26:155–181

Valougeorgis D, Naris S (2003) Acceleration schemes of the discrete velocity method: gaseous flows in rectangular microchannels. SIAM J Sci Comput 25:534–552

Varoutis S, Naris S, Hauer V, Day C, Valougeorgis D (2009) Computational and experimental study of gas flows through long channels of various cross sections in the whole range of the Knudsen number. J Vac Sci Technol A 27:89–100

Wagner W (1992) A convergence proof for Bird direct simulation Monte Carlo method for the Boltzmann equation. J Stat Phys 66:1011–1044

Zohar Y, Lee SYK, Lee WY, Jiang L, Tong P (2002) Subsonic gas flow in a straight and uniform microchannel. J Fluid Mech 472:125–151